Line-Start Permanent-Magnet Motor Single-Phase Steady-State Performance Analysis

T. J. E. Miller, *Fellow, IEEE*, Mircea Popescu, *Member, IEEE*, Calum Cossar, Malcolm McGilp, Giovanni Strappazzon, Nicola Trivillin, and Roberto Santarossa

***Abstract*—This paper describes an efficient calculating procedure for the steady-state operation of a single-phase line-start capacitor-run permanent-magnet motor. This class of motor is beginning to be applied in hermetic refrigerator compressors as a high-efficiency alternative to either a plain induction motor or a full inverter-fed drive. The calculation relies on a combination of reference-frame transformations including symmetrical components to cope with imbalance, and *dq* axes to cope with saliency. Computed results are compared with test data. The agreement is generally good, especially in describing the general properties of the motor. However, it is shown that certain important effects are beyond the limit of simple circuit analysis and require a more complex numerical analysis method.**

***Index Terms*—AC motors, capacitor motors, permanent-magnet (PM) motors, steady-state performance.**

I. Introduction

THE line-start permanent-magnet (PM) motor is a synchronous hybrid PM/reluctance brushless motor that is being developed for applications including compressors and others that require a high-efficiency alternative to the induction motor. These are often capacitor motors fed from a single-phase supply, as is the motor in Fig. 1 [1]. In common with induction motors for such applications, there are two phase windings, the main and auxiliary, and both have an approximately sinusoidal distribution of turns in a concentric layout, Fig. 2.

The history of these motors can be traced back at least 50 years, and it is closely interwoven with that of the synchronous reluctance motor. From the 1960s onwards, analysis methods were developed not only for steady-state operation, but also for the starting, the asynchronous performance, the pull-in performance, and the stability, mostly for polyphase versions which in many cases were "line-started" on to a voltage-source inverter with no shaft position feedback [7]–[12]. Very few papers have focused on the single-phase capacitor motor operating at line frequency, [2]. This paper continues the work started in [4].

Paper IPCSD 03–136, presented at the 2003 Industry Applications Society Annual Meeting, Salt Lake City, UT, October 12–16, and approved for publication in the IEEE TRANSACTIONS ON INDUSTRY APPLICATIONS by the Electric Machines Committee of the IEEE Industry Applications Society. Manuscript submitted for review July 11, 2003 and released for publication December 17, 2003.

T. J. E. Miller, M. Popescu, C. Cossar, and M. McGilp are with the SPEED Laboratory, Department of Electrical Engineering, University of Glasgow, Glasgow G12 8LT, U.K. (e-mail: t.miller@elec.gla.ac.uk; mircea@elec.gla.ac.uk; c.cossar@elec.gla.ac.uk; mal@elec.gla.ac.uk).

G. Strappazzon, N. Trivillin, and R. Santarossa are with ACC Compressors, 33170 Pordenone, Italy (e-mail: giovanni.strappazzon@accomp.it; nicola.trivillin@accomp.it; roberto1.santarossa@electrolux.it).

Digital Object Identifier 10.1109/TIA.2004.824492

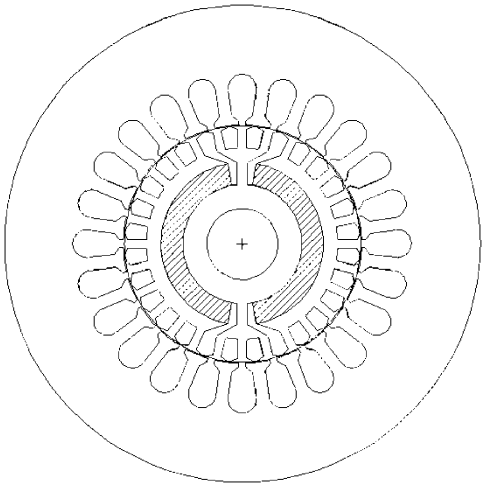

Fig. 1. Single-phase line-start PM motor.

Coil	Go	Ret	Span	Turns
1	1	12	11	130
2	2	11	9	130
3	3	10	7	90
4	4	9	5	74
5	5	8	3	61
6	24	13	-11	130
7	23	14	-9	130
8	22	15	-7	90
9	21	16	-5	74
10	20	17	-3	61

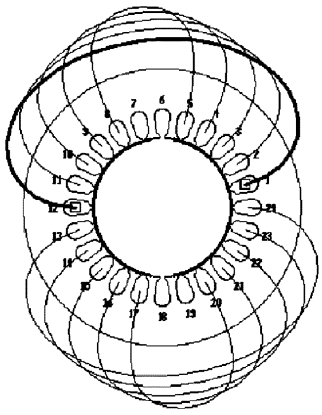

Fig. 2. Winding layout, main phase.

The electrical connections are shown in Fig. 3. The capacitor is connected in series with the auxiliary winding, and the rotation is from the auxiliary to the main. Normally the winding axes are oriented at 90° to one another, but other angles are possible, as shown in Fig. 4.

II. Analysis

A. Reference-Frame Transformations

The analysis follows the sequence of reference frame transformations in Fig. 5, originally published in [4]; see also [5], [6], [15]–[19]. The transformation for current is developed on

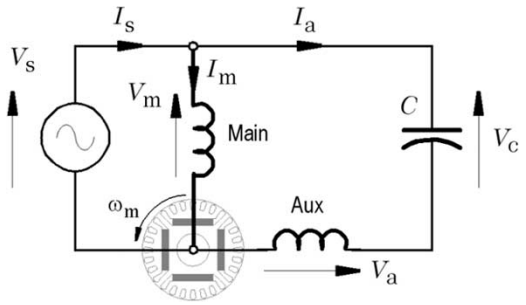

Fig. 3. Electrical connection.

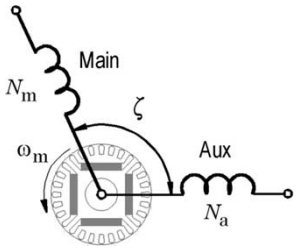

Fig. 4. Nonorthogonal windings.

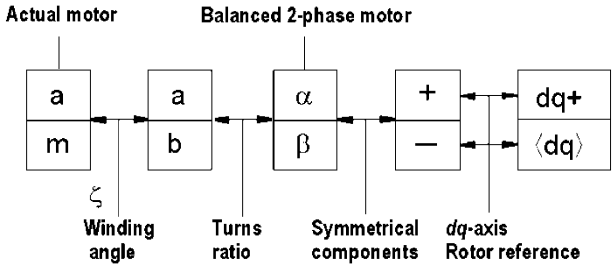

Fig. 5. Reference frame transformations.

the basis of equal magnetomotive force (MMF) on two orthogonal axes. Referring all windings to the auxiliary turns N_a, with $\beta = N_m/N_a$,

$$N_a i_\alpha = N_a i_a + N_m i_m \cos\zeta$$
$$N_a i_\beta = N_m i_m \sin\zeta$$

i.e.,

$$\begin{bmatrix} i_\alpha \\ i_\beta \end{bmatrix} = \begin{bmatrix} 1 & \beta\cos\zeta \\ 0 & \beta\sin\zeta \end{bmatrix} \cdot \begin{bmatrix} i_a \\ i_m \end{bmatrix}, \text{ or } [i_{\alpha,\beta}] = [N][i_{a,m}] \quad (1)$$

with inverse

$$\begin{bmatrix} i_a \\ i_m \end{bmatrix} = \begin{bmatrix} 1 & \text{ctg}\,\zeta \\ 0 & \frac{1}{\beta}\text{csc}\,\zeta \end{bmatrix} \cdot \begin{bmatrix} i_\alpha \\ i_\beta \end{bmatrix} \text{ or } [i_{a,m}] = [N]^{-1}[i_{\alpha,\beta}]. \quad (2)$$

Evidently, $[N]$ is not orthogonal. To maintain power invariance and reciprocal mutual inductances, the voltage transformation must, therefore, be

$$[v_{\alpha,\beta}] = [N_t]^{-1}[v_{a,m}] \quad (3)$$

where "t" means the transpose. The inverse is

$$[v_{a,m}] = [N_t][v_{\alpha,\beta}]. \quad (4)$$

Note that in [4] the nonorthogonal transformation equivalent to (1) is correctly applied to both the voltages and the currents only if $\zeta = 90°$.

The circuit is constrained by the phasor equation

$$\mathbf{V}_s = \mathbf{V}_m = \mathbf{V}_a + \mathbf{Z}_c\mathbf{I}_a. \quad (5)$$

Substituting from (2) and (4) in (5), this constraint is expressed in terms of the $[\alpha,\beta]$ voltages and currents by

$$\mathbf{V}_s = \beta\mathbf{V}_\beta = \mathbf{V}_\alpha + \mathbf{Z}_c\mathbf{I}_\alpha. \quad (6)$$

Symmetrical components $\mathbf{V}_1$, $\mathbf{V}_2$ and $\mathbf{I}_1$, $\mathbf{I}_2$ are introduced by the following mapping from the balanced $[\alpha,\beta]$ machine:

$$\begin{bmatrix} \mathbf{V}_1 \\ \mathbf{V}_2 \end{bmatrix} = \frac{1}{\sqrt{2}} \begin{bmatrix} 1 & \text{j} \\ 1 & -\text{j} \end{bmatrix} \cdot \begin{bmatrix} \mathbf{V}_\alpha \\ \mathbf{V}_\beta \end{bmatrix}, \text{ i.e., } [\mathbf{V}_{1,2}] = [\boldsymbol{S}][\mathbf{V}_{\alpha,\beta}] \quad (7)$$

with inverse

$$\begin{bmatrix} \mathbf{V}_\alpha \\ \mathbf{V}_\beta \end{bmatrix} = \frac{1}{\sqrt{2}} \begin{bmatrix} 1 & 1 \\ -\text{j} & \text{j} \end{bmatrix} \cdot \begin{bmatrix} \mathbf{V}_1 \\ \mathbf{V}_2 \end{bmatrix}, \text{ i.e., } [\mathbf{V}_{\alpha,\beta}] = [\boldsymbol{S}]^{-1}[\mathbf{V}_{1,2}]. \quad (8)$$

Since the complex transformation matrix $[\boldsymbol{S}]$ is unitary, i.e. $[\boldsymbol{S}_t^*] = [\boldsymbol{S}]^{-1}$, power invariance will be maintained if the same transformations are applied to the currents in both directions, i.e.,

$$[\mathbf{I}_{1,2}] = [\boldsymbol{S}][\mathbf{I}_{\alpha,\beta}] \quad (9)$$

with inverse

$$[\mathbf{I}_{\alpha,\beta}] = [\boldsymbol{S}]^{-1}[\mathbf{I}_{1,2}]. \quad (10)$$

Substituting from (8) and (10) in (6), we get

$$\sqrt{2}\beta\mathbf{V}_\beta = \mathbf{a}_1\mathbf{V}_1 + \mathbf{a}_2\mathbf{V}_2 \quad (11)$$

where

$$\mathbf{a}_1 = 1 + \frac{\mathbf{Z}_c}{\mathbf{Z}_1}; \quad \mathbf{a}_2 = 1 + \frac{\mathbf{Z}_c}{\mathbf{Z}_2} \quad (12)$$

and

$$\mathbf{V}_1 = \mathbf{Z}_1\mathbf{I}_1; \quad \mathbf{V}_2 = \mathbf{Z}_2\mathbf{I}_2. \quad (13)$$

$\mathbf{Z}_1$ is the positive-sequence impedance and $\mathbf{Z}_2$ the negative-sequence impedance. Combining (11) with (8), we get

$$\mathbf{V}_1 = \frac{\sqrt{2}}{\beta}\frac{\beta + \text{j}\mathbf{a}_2}{\mathbf{a}_1 + \mathbf{a}_2}\mathbf{V}_m \quad (14)$$

and

$$\mathbf{V}_2 = \frac{\sqrt{2}}{\beta}\frac{\beta - \text{j}\mathbf{a}_1}{\mathbf{a}_1 + \mathbf{a}_2}\mathbf{V}_m. \quad (15)$$

Once $\mathbf{I}_1$ and $\mathbf{I}_2$ are known (from the solution described later), the actual winding currents follow:

$$\mathbf{I}_m = \frac{1}{\beta}\mathbf{I}_\beta = \frac{-\text{j}}{\sqrt{2}\beta}[\mathbf{I}_1 - \mathbf{I}_2] \quad (16)$$

and

$$\mathbf{I}_a = \mathbf{I}_\alpha = \frac{1}{\sqrt{2}}[\mathbf{I}_1 + \mathbf{I}_2]. \quad (17)$$

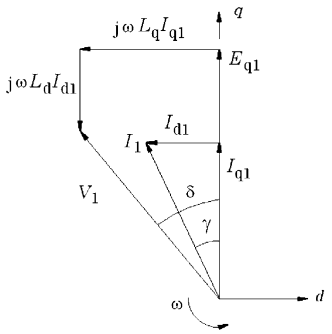

Fig. 6. Positive-sequence phasor diagram.

B. Solution of the Positive-Sequence System

The positive-sequence system must be solved to obtain $\mathbf{Z}_1$. If $\mathbf{V}_1$ is assumed known, the phasor diagram can be used to find $\mathbf{I}_1$, and since the positive-sequence system involves a forward-rotating ampere-conductor distribution synchronized with the rotor, it is convenient to solve the phasor diagram in dq axes as shown in Fig. 6. For reasons explained later, it is assumed that the load angle δ and the positive-sequence voltage $\mathbf{V}_1$ are known, and the diagram is solved for $\mathbf{I}_1$. With p pole pairs, the torque is given in two components: the PM alignment torque,

$$T_{\rm pma} = \frac{p}{\omega} E_{\rm q1} I_{\rm q1} \tag{18}$$

and the synchronous reluctance torque

$$T_{\rm rel} = \frac{p}{\omega}(X_{\rm d} - X_{\rm q}) I_{\rm d1} I_{\rm q1}. \tag{19}$$

Note that the "number of phases" does not appear in these equations. There is only one positive-sequence "phase" and it accounts for all the positive-sequence power.

When the magnet rotates on open-circuit it generates the electromotive force (EMF) $\mathbf{E}_{\rm m} = {\rm j}\omega N_{\rm m}\Phi$ in the main winding and $\mathbf{E}_{\rm a} = -\omega N_{\rm a}\Phi$ in the auxiliary winding, where Φ is the fundamental magnet flux/pole. Thus, $\mathbf{E}_{\rm a} = +{\rm j}\mathbf{E}_{\rm m}/\beta$. From (3) we get $\mathbf{E}_\alpha = \mathbf{E}_{\rm a} = +{\rm j}\mathbf{E}_{\rm m}/\beta$ and $\mathbf{E}_\beta = \mathbf{E}_{\rm m}/\beta$. Then from (7)

$$\mathbf{E}_1 = \frac{1}{\sqrt{2}}[\mathbf{E}_\alpha + \mathbf{E}_\beta] = {\rm j}\sqrt{2}\frac{\mathbf{E}_{\rm m}}{\beta}. \tag{20}$$

Thus, if $E_{\rm q1}$ is normally calculated for the main winding ($N_{\rm m}$ turns), it must be scaled by $\sqrt{2}/\beta$ to get the positive-sequence value to be used in Fig. 2.

Note that the dq axes in Fig. 6 can be interpreted as a further reference-frame transformation into a d-axis and a q-axis circuit, as is apparent from the equations used to solve this diagram. As they are standard and self-evident from the diagram, they are not repeated here. This transformation is depicted in Fig. 5.

C. Solution of the Negative-Sequence System

The negative-sequence system must be solved to obtain $\mathbf{Z}_2$. For this purpose the motor equations are written in dq axes fixed to the rotor, and solved for a slip $s = 2$. (See [4]). For the stator we have

$$\begin{aligned} v_{\rm d} &= R_{\rm d} i_{\rm d} + \mathbf{p}\psi_{\rm d} - \mathbf{p}\theta.\psi_{\rm q} \\ v_{\rm q} &= R_{\rm q} i_{\rm q} + \mathbf{p}\psi_{\rm q} + \mathbf{p}\theta.\psi_{\rm d} \end{aligned} \tag{21}$$

where $R_{\rm d} = R_{\rm q} = R$, the stator resistance/phase. Evidently all the impedances in this system, including $\mathbf{Z}_2$, are referred to a winding with a particular number of turns. It is usual to calculate impedances referred to the main winding with $N_{\rm m}$ turns. If both windings have the same total copper cross section, we can write $R_{\rm a} = R_{\rm m}/\beta^2$ where $R_{\rm m}$ is the resistance of the main winding, and $R_{\rm a}$ the resistance of the auxiliary. The resistance matrix of the $[a, m]$ machine is then

$$[R_{\rm a,m}] = \begin{bmatrix} R_{\rm a} & 0 \\ 0 & R_{\rm m} \end{bmatrix} = \begin{bmatrix} \frac{R_{\rm m}}{\beta^2} & 0 \\ 0 & R_{\rm m} \end{bmatrix}. \tag{22}$$

Using the transformations (1) and (3), if we first write

$$[V_{\rm a,m}] = [R_{\rm a,m}][I_{\rm a,m}] \tag{23}$$

we get

$$\begin{aligned} [V_{\alpha,\beta}] &= [C_{\rm t}]^{-1}[V_{\rm a,m}] \\ &= [C_{\rm t}]^{-1}[R_{\rm a,m}][I_{\rm a,m}] \\ &= [C_{\rm t}]^{-1}[R_{\rm a,m}][C]^{-1}[I_{\alpha,\beta}] \end{aligned} \tag{24}$$

from which

$$[R_{\alpha,\beta}] = [C_{\rm t}]^{-1}[R_{\rm a,m}][C]^{-1} = \begin{bmatrix} \frac{R_{\rm m}}{\beta^2} & 0 \\ 0 & \frac{R_{\rm m}}{\beta^2} \end{bmatrix}. \tag{25}$$

The same process is applied to obtain $[R_{1,2}]$ from $[R_{\alpha,\beta}]$ using the transformations $[\boldsymbol{S}]$ and $[\boldsymbol{S}]^{-1}$ in (7) and (10), thus,

$$[R_{1,2}] = [\boldsymbol{S}][R_{\alpha,\beta}][\boldsymbol{S}]^{-1} = [R_{\alpha,\beta}]. \tag{26}$$

From this it appears that in the solution of the negative-sequence system all resistances and inductances should be referred to the auxiliary winding: for example if they initially calculated for the main winding turns $N_{\rm m}$, they should be scaled by $1/\beta^2$.

The voltage and current must also be scaled correctly. The negative-sequence voltage is not known *a priori*, but suppose the value is $\mathbf{V}_2$. Considering the negative-sequence system in isolation, we can set $\mathbf{V}_1 = 0$. Then, from (8),

$$\mathbf{V}_\alpha = \frac{1}{\sqrt{2}}\mathbf{V}_2 \quad \text{and} \quad \mathbf{V}_\beta = \frac{\rm j}{\sqrt{2}}\mathbf{V}_2. \tag{27}$$

Then, from (4),

$$\mathbf{V}_{\rm a} = \mathbf{V}_\alpha = \frac{1}{\sqrt{2}}\mathbf{V}_2 \quad \text{and} \quad \mathbf{V}_{\rm m} = \beta\mathbf{V}_\beta = \frac{{\rm j}\beta}{\sqrt{2}}\mathbf{V}_2. \tag{28}$$

From (28) it appears that if the voltages to be used in the negative-sequence system are to be referred to the auxiliary winding, they must be scaled from $\mathbf{V}_2$ by $1/\sqrt{2}$.

It is now possible to proceed with the solution of (21) under asynchronous conditions with a slip of $s = 2$. Relative to a balanced two-phase $[\alpha, \beta]$ machine with $N_{\rm a}$ turns in both windings, the dq voltages can be identified as

$$\begin{bmatrix} v_{\rm d} \\ v_{\rm q} \end{bmatrix} = \begin{bmatrix} \cos\theta & \sin\theta \\ -\sin\theta & \cos\theta \end{bmatrix} \cdot \begin{bmatrix} v_\alpha \\ v_\beta \end{bmatrix}. \tag{29}$$

Now, let the $[\alpha, \beta]$ machine be supplied with positive-sequence voltages

$$\begin{aligned} v_\alpha &= V_{\rm pk}\cos\omega t \\ v_\beta &= V_{\rm pk}\sin\omega t \end{aligned} \tag{30}$$

in which v_α leads v_β. The negative-sequence behavior will be imposed by rotating the rotor backward relative to the rotating ampere-conductor distribution established by these voltages. If we have

$$\theta = (1-s)\omega t \tag{31}$$

and substitute (30) and (31) in (29), we get

$$v_\mathrm{d} = V_\mathrm{pk}\cos s\omega t \quad \text{and} \quad v_\mathrm{q} = V_\mathrm{pk}\sin s\omega t \tag{32}$$

which shows that with positive slip, v_d leads v_q. The rotor is slipping backward relative to the stator ampere-conductor distribution, which is rotating at synchronous speed according to (30). For the purpose of analysis with (21) we can represent v_d and v_q as phasor values at the slip frequency $s\omega$:

$$\mathbf{V}_\mathrm{d} = V_\mathrm{pk} \quad \text{and} \quad \mathbf{V}_\mathrm{q} = -\mathrm{j}V_\mathrm{pk}. \tag{33}$$

Equations (21) are now expressed in phasor terms

$$\begin{aligned}\mathbf{V}_\mathrm{d} &= R_\mathrm{d}\mathbf{I}_\mathrm{d} + \mathrm{j}s\omega\Psi_\mathrm{d} - (1-s)\omega\Psi_\mathrm{q}\\ \mathbf{V}_\mathrm{q} &= R_\mathrm{q}\mathbf{I}_\mathrm{q} + \mathrm{j}s\omega\Psi_\mathrm{q} - (1-s)\omega\Psi_\mathrm{d}\end{aligned} \tag{34}$$

in which

$$\begin{aligned}\Psi_\mathrm{d} &= L_\mathrm{d}(\mathrm{j}s\omega)\mathbf{I}_\mathrm{d}\\ \Psi_\mathrm{q} &= L_\mathrm{q}(\mathrm{j}s\omega)\mathbf{I}_\mathrm{q}.\end{aligned} \tag{35}$$

The synchronous inductances $L_\mathrm{d}(\mathrm{j}s\omega)$ and $L_\mathrm{q}(\mathrm{j}s\omega)$ are functions of frequency because of the coupled rotor circuits in each axis. We can derive expressions for $L_\mathrm{d}(\mathrm{j}s\omega)$ and $L_\mathrm{q}(\mathrm{j}s\omega)$ as follows. First the stator flux linkage is written in the d and q axes as

$$\begin{aligned}\Psi_\mathrm{ds} &= L_\mathrm{ds}\mathbf{I}_\mathrm{ds} + M_\mathrm{d}\mathbf{I}_\mathrm{dr}\\ \Psi_\mathrm{dr} &= M_\mathrm{d}\mathbf{I}_\mathrm{ds} + L_\mathrm{dr}\mathbf{I}_\mathrm{dr}\end{aligned} \tag{36}$$

where L_dr is the rotor self-inductance in the d axis referred to the same circuit as L_ds for the stator, and similarly for L_qr and L_qs. The mutual inductance between these circuits is

$$M_\mathrm{d} = k_\mathrm{d}\sqrt{L_\mathrm{ds}L_\mathrm{dr}} \tag{37}$$

where k_d is the d-axis coupling coefficient; $k_\mathrm{d} < 1$. Similar equations can be written for M_q.

The rotor circuits are short circuited, so that in the d axis, for example,

$$\begin{aligned}0 &= R_\mathrm{dr}\mathbf{I}_\mathrm{dr} + \mathrm{j}s\omega\Psi_\mathrm{dr}\\ &= R_\mathrm{dr}\mathbf{I}_\mathrm{dr} + \mathrm{j}s\omega(M_\mathrm{d}\mathbf{I}_\mathrm{ds} + L_\mathrm{dr}\mathbf{I}_\mathrm{dr}).\end{aligned} \tag{38}$$

This equation can be used to eliminate $\mathbf{I}_\mathrm{dr}$ from (36). First,

$$\mathbf{I}_\mathrm{dr} = \frac{-\mathrm{j}s\omega M_\mathrm{d}}{R_\mathrm{dr} + \mathrm{j}s\omega L_\mathrm{dr}}\mathbf{I}_\mathrm{ds} \tag{39}$$

then after some manipulation

$$L_\mathrm{ds}(\mathrm{j}s\omega) = L_\mathrm{ds}\left[1 - \frac{\mathrm{j}s\omega {k_\mathrm{d}}^2 T_\mathrm{d}}{1 + \mathrm{j}s\omega T_\mathrm{d}}\right] \tag{40}$$

with

$$T_\mathrm{d} = \frac{L_\mathrm{dr}}{R_\mathrm{dr}} \tag{41}$$

the so-called "open-circuit" rotor time constant. Equations similar to (40) and (41) can be written for the q-axis. At any particular slip frequency $L_\mathrm{d}(\mathrm{j}s\omega)$ and $L(\mathrm{j}s\omega)$ are calculated and when the rotor current is eliminated using (39), (34) and (35) become

$$\begin{aligned}(R_\mathrm{d} + \mathrm{j}s\omega L_\mathrm{d})\mathbf{I}_\mathrm{d} - (1-s)\omega L_\mathrm{q}\mathbf{I}_\mathrm{q} - \mathbf{V}_\mathrm{d} &= 0\\ (1-s)\omega L_\mathrm{d}\mathbf{I}_\mathrm{d} + (R_\mathrm{q} + \mathrm{j}s\omega L_\mathrm{q})\mathbf{I}_\mathrm{q} - \mathbf{V}_\mathrm{q} &= 0\end{aligned} \tag{42}$$

with the voltages $\mathbf{V}_\mathrm{d}$ and $\mathbf{V}_\mathrm{q}$ given by (33). These can be solved for $\mathbf{I}_\mathrm{d}$ and $\mathbf{I}_\mathrm{q}$, whence Ψ_d and Ψ_q follow from (35), and the negative-sequence impedance is obtained as

$$\mathbf{Z}_2 = \frac{\mathbf{V}_\mathrm{d} + \mathrm{j}\mathbf{V}_\mathrm{q}}{\mathbf{I}_\mathrm{d} + \mathrm{j}\mathbf{I}_\mathrm{q}}. \tag{43}$$

The average negative-sequence torque is also computed as

$$T_\mathrm{ns} = p\,\mathrm{Re}\left[{\Psi_\mathrm{d}}^*\mathbf{I}_\mathrm{q} - {\Psi_\mathrm{q}}^*\mathbf{I}_\mathrm{d}\right]. \tag{44}$$

Again, as in (19), the number of "phases" does not appear in (44) because there is only one "phase" in the negative-sequence system. The analysis in this section is taken from Adkins [20], and the relationship between the dq axes and the negative sequence component is depicted in Fig. 5, in which the symbol $\langle\rangle$ reflects the fact that $\mathbf{Z}_2$ is the average between the slip-dependent d- and q-axis impedances. The negative-sequence system of equations can be used at other values of slip s, so it can also be applied to calculate the asynchronous cage torque. When added to the short-circuit magnet braking torque, it provides a means for calculating the entire asynchronous torque/speed curve, which is important in the analysis of starting.

D. Combined Solution of the Positive- and Negative-Sequence Systems

So far we have treated the positive- and negative-sequence systems separately. In actual operation the link between them is provided by (14), which "ties" the positive-sequence voltage $\mathbf{V}_1$ to the supply voltage $\mathbf{V}_\mathrm{m}$ and (15), which does the same for the negative-sequence voltage $\mathbf{V}_2$. Only a single control parameter is needed to set the "level of operation", and the one chosen is the positive-sequence load angle δ (see Fig. 6). The algorithm is shown in Fig. 7. The total torque is obtained by adding (18), (19) and (44). The rotor copper loss is given by

$$W_\mathrm{CuR} = s\omega T_\mathrm{ns}. \tag{45}$$

Once $\mathbf{I}_1$ and $\mathbf{I}_2$ are known, the phase currents can be recovered using (10) followed by (2), and then the line current, the power factor, and the electrical power follow straightforwardly.

For the negative-sequence system it is necessary to know the coupling coefficients k_d, k_q and the time constants T_d and T_q, Given the high value of slip ($s = 2$), it seems reasonable to assume that the cage currents screen the interior of the rotor to

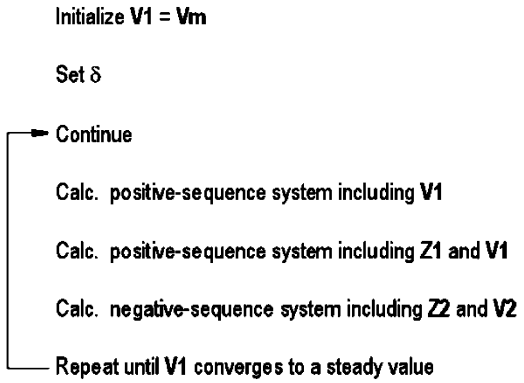

Fig. 7. Combined solution.

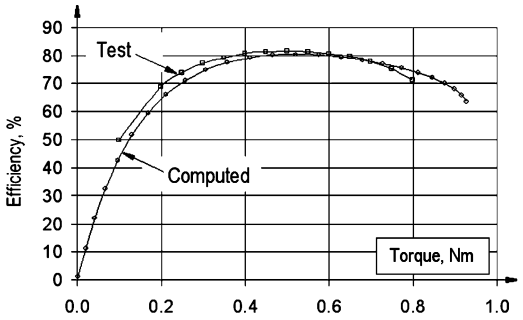

Fig. 8. Efficiency, motor A; computed versus test.

such an extent that the effective leakage inductance and referred rotor resistances $R_{\rm dr}$ and $R_{\rm qr}$ are the same in both axes. Then,

$$L_{\rm dr} = L_{\rm md} + L_2 \quad L_{\rm qr} = L_{\rm mq} + L_2 \tag{46}$$

where L_2 is the rotor leakage inductance and $L_{\rm md}$ and $L_{\rm mq}$ are the magnetizing inductances,

$$L_{\rm md} = L_{\rm ds} - L_1 \quad L_{\rm mq} = L_{\rm qs} - L_1. \tag{47}$$

$L_{\rm ds}$ and $L_{\rm qs}$ are the synchronous inductances in the two axes, and L_1 is the stator leakage inductance. The leakage inductances L_1 and L_2 and the referred rotor resistance are calculated by standard methods as though the motor were an induction motor. A more detailed method which differentiates d- and q-axis values will be published later.

III. Test Data

Extensive dynamometer testing has been conducted on a two-pole 50-Hz 220-V motor designed for a mechanical power output in the region of 200 W. The motor has ferrite magnets and a rotor with 28 cage bars and 24 stator slots, [1].

Here, test data is compared with a computation for two versions of the motor, A and B. Both motors have the same auxiliary/main turns ratio (0.7). Motor B has about 30% more turns, with a comparable slot-fill factor, and helps to show the effect of a change in supply voltage.

Fig. 8 shows the efficiency as a function of load for motor A, and Fig. 9 for motor B. Agreement is close especially over the range that includes maximum efficiency. The test and computed curves deviate at high load, probably because of increasing saturation of the q axis. The computed results are sensitive to $X_{\rm q}$,

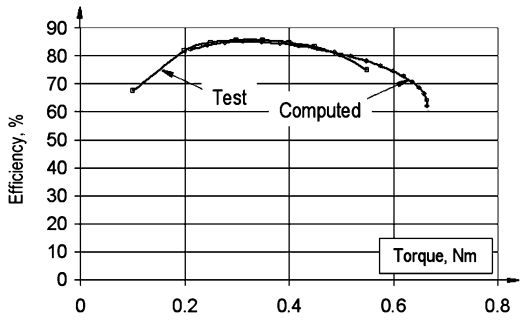

Fig. 9. Efficiency, motor B; computed versus test.

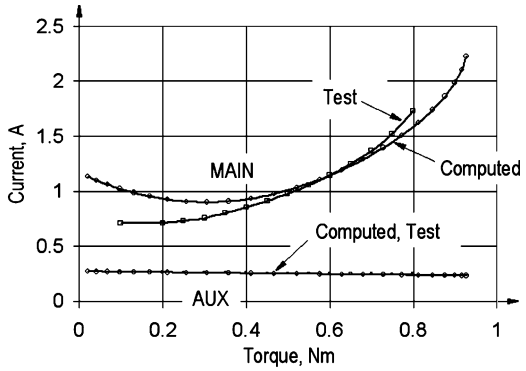

Fig. 10. Main and auxiliary currents of motor A.

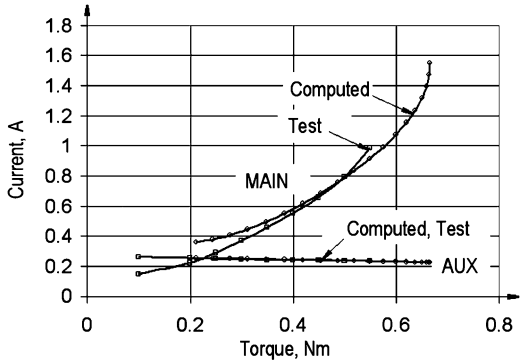

Fig. 11. Main and auxiliary currents of motor B.

and all points in Figs. 8–11 were computed with fixed values of all the motor parameters, but for more accurate calculations it may be desirable to calibrate or adjust $X_{\rm q}$ and $X_{\rm d}$ using finite-element analysis, an example of which is shown in Fig. 12. The key sections that determine the effect of saturation can be identified visually in this diagram.

Saturation of the magnetic circuit is particularly complex in this motor type: different sections of the machine saturate independently, causing large and sometimes time-varying changes in equivalent-circuit parameters such as inductances $X_{\rm d}$ and $X_{\rm q}$ and EMF $(E_{\rm q1})$. Accordingly, two series of finite-element calculations were carried out, one with current only in the d axis and the other with current only in the q axis. For each solution, $X_{\rm d}$ and $X_{\rm q}$ were obtained as in [21]. As an illustrative example the results for Motor B are given in Fig. 13 which expresses $X_{\rm d}$ as a function of $I_{\rm d}$ with $I_{\rm q} = 0$, and $X_{\rm q}$ as a function of $I_{\rm q}$ with $I_{\rm d} = 0$. In all cases it is assumed that $E_{\rm q1}$ is constant, as in [1].

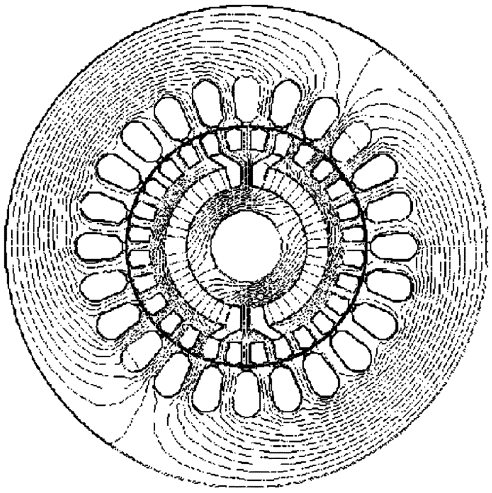

Fig. 12. Finite-element computation.

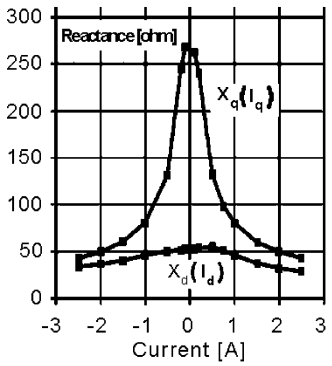

Fig. 13. Variation of X_d vs. I_d with $I_q = 0$, and of X_q versus I_q with $I_d = 0$, calculated using finite-element [21] data with constant E.

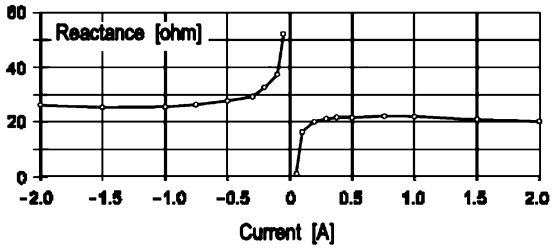

Fig. 14. X_d versus I_d with $I_q = 2.0$ A (peak).

Fig. 13 shows a huge variation of 6:1 in $X_{\rm q}$ and almost 2:1 in $X_{\rm d}$.

Calculations with current flowing simultaneously in both axes show that $X_{\rm d}$ is affected by $I_{\rm q}$, being increased when $I_{\rm d} < 0$ and decreased when $I_{\rm d} > 0$, with $I_{\rm q} > 0$. An example is shown in Fig. 14 which is computed for $I_{\rm q} = 2.0$ A (peak), and varying $I_{\rm d}$. The discontinuity at $I_{\rm d} = 0$ is explained in connection with the "frozen permeability" method in [21]. It can be attributed to an error or variation ΔE from the open-circuit value $E_{\rm q1}$

$$X_{\rm d} = \frac{V_{\rm q} - (E_{\rm q1} + \Delta E)}{I_{\rm d}}. \tag{48}$$

If E is assumed constant and equal to $E_{\rm q1}$, the value of $X_{\rm d}$ that will be inferred by using only the first term of (48) is in error by $\Delta E/I_{\rm d}$, which is indefinite when $I_{\rm d} = 0$. Evidently, the effect of cross saturation is that E depends on the current components $I_{\rm d}$ and $I_{\rm q}$ as do $X_{\rm d}$ and $X_{\rm q}$. Note that although the finite-element method can be used to calculate $E_{\rm q1}$, $X_{\rm d}$ and $X_{\rm q}$ for use in the phasor diagram, this method applies only to motors that have sinedistributed windings and sinusoidal waveforms of EMF, current, and terminal voltage. An important and accurate alternative to estimate the electromagnetic torque is the flux-MMF diagram [21].

In the previous sections it was emphasized that for a correct implementation of the symmetrical components theory, all the equivalent circuit parameters have to be referred to one of the stator windings: main or auxiliary (as in the actual approach). If the stator windings have similar distribution (coils span, total number of coils, etc.) when computing or measuring the dq–axes synchronous reactances, there is no significant variation in the predicted results regardless of the choice for the reference stator winding. However, when the differences between stator winding are insufficiently described just by using the turns ratio, one should use only the reference winding for inductance computation and/or estimation through experimental data. This is justified by the different saturation levels that might occur when the main or the auxiliary winding is used as reference.

Motor B has a higher maximum efficiency and this efficiency occurs at lower load. The flatness of the efficiency curve is better for motor A. In both cases the losses are dominated by copper loss, the iron loss and friction loss being quite small (in the region of 14 W combined total).

In both Figs. 10 and 11 the computed auxiliary current is close to the measured value at all loads, but it must be said that this branch of the circuit is dominated by the capacitor impedance, which is accurately known. The main winding current shows good agreement over the range near maximum efficiency, but less good at extremes of high or low load. Interestingly, the main winding current increases roughly quadratically with load, while the auxiliary current remains almost constant.

The operation is summarized in the phasor diagram of Fig. 15 which shows not only the main and auxiliary voltages and currents, but also the capacitor voltage, the open-circuit EMF $\mathbf{E}_{\rm q1}$ of the main winding, and the symmetrical components $\mathbf{V}_1$, $\mathbf{V}_2$, $\mathbf{I}_1$ and $\mathbf{I}_2$. Here the auxiliary current is small, so $\mathbf{I}_1$ and $\mathbf{I}_2$ are almost equal and opposite, as would be expected from (1) and (9). The motor is operating almost as a pure single-phase motor. Evidently $\mathbf{Z}_2$ is small, so the negative-sequence voltage and the backward rotating flux are both small, while the positive-sequence voltage $\mathbf{V}_1$ is essentially applied to the main winding apart from the $\mathrm{j}\sqrt{2}$ factor from (7).

The positive- and negative-sequence effects can be superimposed only if the stator windings are assumed to have the same copper weight. Thus, for a similar main and auxiliary winding distribution we actually assume that the main/auxiliary turns ratio (β) is equal to the conductors area ratio (aux/main). Physically, for the tested motors this would have meant that as $\beta > 1$, the auxiliary winding should have been realized with a higher diameter conductor than the main winding. However, due to the slot area limits the actual auxiliary winding was constructed using a lower diameter conductor than the main winding. This

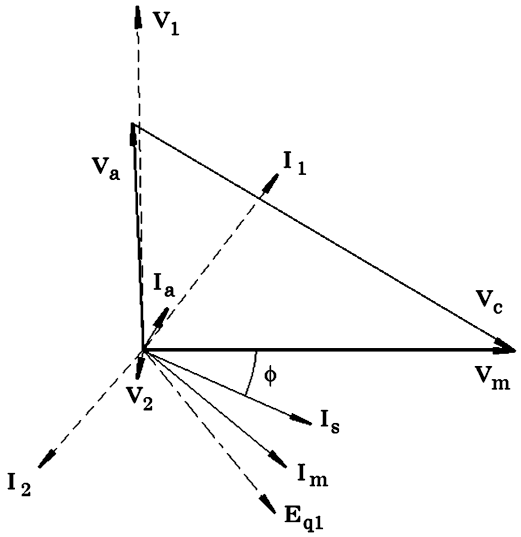

Fig. 15. Typical phasor diagram.

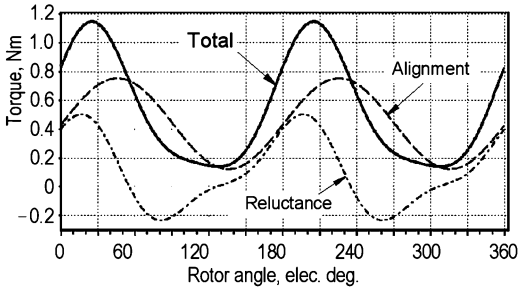

Fig. 16. Torque waveforms.

may represent an important error source if the turns ratio exhibits values much higher or lower than 1.

The waveforms of the various torque components can also be readily extracted from the computed results, as shown in Fig. 16. When the motor is perfectly balanced with no negative-sequence current, the torque is constant, but any degree of imbalance introduces both second and fourth harmonic torque components. The negative-sequence torque is very small and does not appear in Fig. 16.

For comparison, in Fig. 17 the positive- and negative-sequence torques are illustrated using appropriate scale factors. It can be observed that the positive-sequence torque is almost two orders higher than the negative-sequence torque. From (15) it follows that if the auxiliary capacitive impedance $(\mathbf{Z}_{\mathrm{C}})$ is much higher than the motor reactances (case of the tested motors), the negative-sequence voltage $\mathbf{V}_2$ is just a fraction of the positive-sequence voltage $\mathbf{V}_1$. Consequently, the negative-sequence torque is minimized. It is important to observe that a lower value of the negative-sequence voltage does not guarantee a low value for the negative-sequence current $(\mathbf{I}_2)$ which is translated in rotor cage losses (45). This means that even though the air-gap electromagnetic torque is not substantially diminished by the negative-sequence torque, the motor performance can be worsened because of the poorer efficiency. Thus, the minimization of negative-sequence voltage should be observed in connection with a similar minimization of the negative-sequence current.

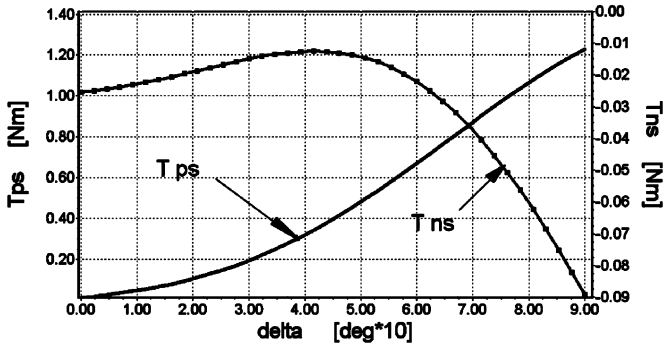

Fig. 17. Positive (T ps) and negative (T ns) sequence torque.

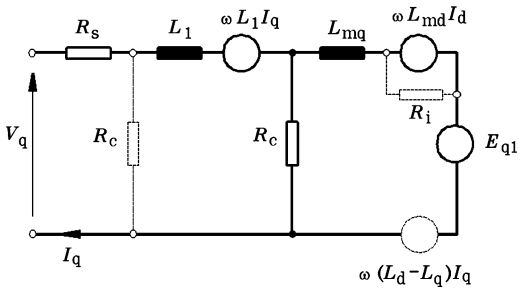

Fig. 18. Incorporating a resistance for core loss.

If the stator windings have the same copper weight, then based on (14)–(17) one can demonstrate that the motor can be balanced (negative sequence voltage and current equals zero) when the current density in the main winding equals the current density in the auxiliary winding. Alternatively, the balanced conditions can be achieved if the ratio of the stator currents amplitude equals the effective turns ratio.

IV. Circuit Representation and Effect of Core Loss

In polyphase induction motors it is usual to represent the core loss approximately by a resistor in the equivalent circuit, in parallel with the magnetizing inductance. This is possible also in the polyphase PM motor, but in the single-phase motor there are, in effect, separate equivalent circuits for the positive- and negative-sequence fields, and even for the d and q axes. In cases where the iron loss is small, a high level of precision may not be necessary, and one simple strategy is to incorporate the iron loss resistor in the positive-sequence circuit only, on the grounds that the backward field is normally small.

Fig. 18 shows the general form of three alternative core loss models: L includes a single resistor R_{c} at the phase terminals [13]; T includes a single resistor R_{c} in parallel with the magnetizing inductance [9]; and Ti adds a further current-dependent resistor R_{i} in parallel with the respective synchronous inductances in the two axes [22]. (Fig. 15 shows only the q-axis equivalent circuit; the d-axis circuit is similar but without E_{q1}).

The effect of these alternative models is shown in Fig. 19, in terms of the available torque as a function of the load angle. As a general observation, circuit L predicts a lower torque for the whole range of load angles; circuit T predicts a lower torque value for load angles between zero and pull-out; conversely, circuit Ti predicts higher torque for this range.

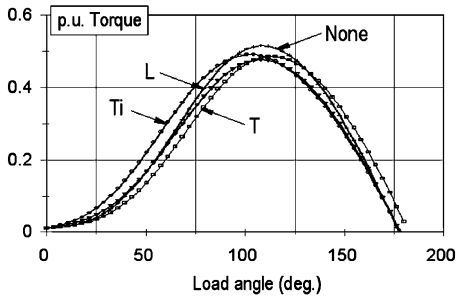

Fig. 19. Effect of core loss resistance on load curve.

The estimation of the iron loss resistor can be made analytically with empirical models or by finite-element methods [30], or using specific test data [22], [30], [31].

For fractional horsepower motors, when high quality lamination steel is employed, the core losses represent approximately 2%–5% of the input power. However, it may be necessary for the design engineer to address the core losses minimization issue for a rated power higher than 1 kW or specific materials (e.g., soft magnetic composite) are used.

V. Design Constraints

A characteristic of the line-start PM motors is that certain parameters would improve the starting and synchronization capabilities [1]–[4], [12] but affect the steady-state motor performance, while other parameters would improve the motor efficiency [18], [23] but worsen starting operation.

Specifically, the cage rotor and the magnets material and configuration have to be optimized. In Section III it was stated that for low-power applications, at synchronous speed the single-phase line-start PM motor can be easily operated close to balanced conditions. This task is achieved by the appropriate selection of the run capacitor. Thus, the main loss source is represented by the copper losses. If the stator copper losses can be minimized by increasing the number of turns, the rotor copper losses are dependent on the cage resistance. A lower resistance cage (deep bars, low number of bars) would seem to be the obvious solution. Besides minimizing the rotor copper losses, lower rotor resistance means improved synchronization capability [12] as the slope of the cage torque characteristic will be very steep. The drawback is that the starting cage torque [1] is directly dependent on the cage rotor resistance. Consequently, the starting torque criterion will impose the lowest limit of the rotor resistance that would ensure a good starting performance. Also, a uniform distribution of deep bars is not possible due to the presence of buried magnets. Any asymmetry in the rotor cage will be transformed in the classical "dip" around half synchronous speed (Goerges phenomenon) and in important torque oscillations [1] during starting and steady-state operation. Deep rotor bars can be successfully used as flux barriers for the rotor with buried PMs. Several solutions for the rotor cage configuration have been patented [32]–[35]. An optimized cage rotor configuration can be made only by combining analytical and numerical tools with test data.

Another important issue to be addressed in an optimized design is presented by the magnets materials and configuration. As the rotor dimensions are usually imposed, the proper selection of the magnets material and configuration (dimensions) is a challenging task. Using the analytical and numerical modeling tools, and imposing as optimization criterion efficiency versus torque, one can estimate the necessary no-load induced voltage amplitude that corresponds to a maximum efficiency. Considering also the cost criterion, the no-load induced voltage is translated into certain magnet materials and dimensions. For example in the tested motors, the same no-load induced voltage can be achieved using ferrites or NdFeB. Beneficial for the synchronous operation, as a supplementary energy source that increases the overall motor efficiency, the magnets rotation at asynchronous speed determines a so-called "magnet braking torque" [1]–[3], [9]–[12]. The magnet braking torque is proportional with the no-load induced voltage amplitude, so a decrease of this voltage level may be necessary to obtain the motor starting criteria. In a similar way to the cage rotor, any solution that decreases the magnet braking torque, would diminish the maximum efficiency. These design constraints will lead to the optimum number of turns per phase for the stator winding, the optimum air-gap value, and the optimum magnet dimensions and material data. The level of the no-load induced voltage has to be verified for possible demagnetization phenomena that occur during starting. The worst case is when the maximum starting current acts along negative d axis (Fig. 6).

The temperature effect has to be considered as an extra design constraint. If a nonlinear thermal analytical model is used, the final temperature can be predicted. Based on this prediction, the motor parameters that vary with temperature are estimated (windings and cage resistance, PM operation point flux density). A more accurate approach is realized through numerical analysis (i.e., finite-element analysis). Numerical computations are necessary to estimate the magnets demagnetization level due to stator currents and temperature [2]. The computations made in this paper have used a nonlinear analytical thermal model to estimate the final temperature. The results were consistent with the experimental data.

VI. Conclusion

On the practical side, this paper has clearly shown the operation of the single-phase capacitor-run permanent-magnet motor with a high efficiency and power factor. With a small run capacitor (3 μF) the motor operates almost as a pure single-phase motor and, as in the induction motor, the backward field has only a weak effect.

On the theoretical side, the calculation procedure is efficient and succeeds in modeling the main performance characteristics, including the efficiency as a function of load. It provides a useful phasor diagram representation and time waveforms of the torques.

The computation is extremely fast. One load point is computed in less than one second, and all the graphs and performance data are immediately available. Although the accuracy is not perfect, it is possible to calibrate the calculation with adjustment factors, so that the computation can be used with confidence for small design modifications. The speed of computation

also makes it possible to examine the effect of particular parameters quickly and thoroughly, so that one can form an idea of which parameters have the greatest effect on performance. For example, it is found that performance is much more sensitive to X_{q} than to X_{d}. As a result of this, it is clear that, as a matter of design philosophy, attention should be paid to the calculation of an accurate value of X_{q}, and the arrangement of the design to achieve a suitable value.

Future work will include a more sophisticated estimate of the reactances, including differential frequency-dependent synchronous inductances in the two axes. Although the core losses are small, further work is desirable in this area and on the surface losses caused by slotting, because at such high levels every small contribution to efficiency is important.

REFERENCES

[1] M. Popescu, T. J. E. Miller, M. I. McGilp, G. Strappazzon, N. Trivillin, and R. Santarossa, "Line start permanent magnet motor: single-phase starting performance analysis," in *Conf. Rec. IEEE-IAS Annu. Meeting*, 2002, pp. 2499–2506.

[2] R. Carlson, N. Sadowski, S. R. Arruda, C. A. da Silva, and L. von Dokonal, "Single phase line-started permanent magnet motor analysis using finite element method," in *Conf. Rec. IEEE-IAS Annu. Meeting*, 1994, pp. 227–233.

[3] C. M. Stephens, G. B. Kliman, and J. Boyd, "A line-start permanent magnet motor with gentle starting behavior," in *Conf. Rec. IEEE-IAS Annu. Meeting*, 1998, pp. 371–379.

[4] T. J. E. Miller, "Single-phase permanent magnet motor analysis," *IEEE Trans. Ind. Applicat.*, vol. 21, pp. 651–658, May/June 1985.

[5] S. S. L. Chang, "An analysis of unexcited synchronous capacitor motors," *AIEE Trans.*, vol. 70, pp. 1978–1982, 1951.

[6] F. W. Suhr, "Symmetrical components as applied to the single-phase induction motor," *AIEE Trans.*, vol. 64, pp. 651–656, 1945.

[7] K. J. Binns, W. R. Barnard, and M. A. Jabbar, "Hybrid permanent-magnet synchronous motors," *Proc. Inst. Elect. Eng.*, vol. 125, pp. 203–208, Mar. 1978.

[8] J. W. Finch and P. J. Lawrenson, "Synchronous performance of single-phase reluctance motors," *Proc. Inst. Elect. Eng.*, vol. 125, pp. 1350–1356, Dec. 1978.

[9] V. B. Honsinger, "Performance of polyphase permanent magnet machines," *IEEE Trans. Power App. Syst.*, vol. PAS-99, pp. 1510–1518, July 1980.

[10] ——, "The fields and parameters of interior type AC permanent magnet machines," *IEEE Trans. Power App. Syst.*, vol. PAS-101, pp. 867–876, Apr. 1982.

[11] K. Miyashita, S. Yamashita, S. Tanabe, T. Shimozu, and H. Sento, "Development of a high speed 2-pole permanent-magnet synchronous motor," *IEEE Trans. Power App. Syst.*, vol. PAS-99, pp. 2175–2183, Nov./Dec. 1980.

[12] T. J. E. Miller, "Synchronization of line-start permanent magnet motors," *IEEE Trans. Power App. Syst.*, vol. PAS-103, pp. 1822–1828, July 1984.

[13] T. Sebastian, G. R. Slemon, and M. A. Rahman, "Modeling of permanent magnet synchronous motors," *IEEE Trans. Magn.*, vol. 22, pp. 1069–1071, Sept. 1986.

[14] J. O. Ojo and T. A. Lipo, "An improved model for saturated salient-pole synchronous motors," *IEEE Trans. Energy Conversion*, vol. 4, pp. 135–142, Mar. 1989.

[15] T. A. Walls and S. D. Sudhoff, "Analysis of a single-phase induction machine with a shifted auxiliary winding," *IEEE Trans. Energy Conversion*, vol. 11, pp. 681–686, Dec. 1996.

[16] T. J. E. Miller and C. B. Rasmussen, "Extended cross-field theory of the tapped-winding capacitor motor, including iron loss and alternate connections," in *Conf. Rec. IEEE-IAS Annu. Meeting*, 2001, pp. 2275–2279.

[17] ——, "Revolving-field polygon technique for performance prediction of single-phase induction motors," in *Conf. Rec. IEEE-IAS Annu. Meeting*, 2000, pp. 457–462.

[18] I. Boldea, T. Dumitrescu, and S. A. Nasar, "Unified analysis of 1-phase AC motors having capacitors in auxiliary windings," *IEEE Trans. Energy Conversion*, vol. 14, pp. 577–582, Sept. 1999.

[19] B. N. Chaudhari and B. G. Fernandes, "Equivalent circuit of single-phase permanent magnet synchronous motor," in *Proc. IEEE-PES Winter Meeting*, 2001, pp. 1378–1381.

[20] B. Adkins, *The General Theory of Electrical Machines*. London, U.K.: Chapman & Hall, 1964.

[21] T. J. E. Miller, M. Popescu, C. Cossar, M. McGilp, and J. A. Walker, "Calculating the interior permanent-magnet motor," in *Proc. IEEE IEMDC*, 2003, pp. 1181–1187.

[22] A. Consoli and A. Racitti, "Analysis of permanent magnet synchronous motors," *IEEE Trans. Ind. Applicat.*, vol. 27, pp. 350–354, Mar./Apr. 1991.

[23] S. Williamson and A. M. Knight, "Performance of skewed single-phase line-start permanent magnet motors," *IEEE Trans. Ind. Applicat.*, vol. 35, pp. 577–582, May/June 1999.

[24] B. J. Chalmers, G. D. Baines, and A. C. Williamson, "Performance of a line-start single-phase permanent-magnet synchronous motor," in *Proc. Seventh Int. Conf. Electrical Machines and Drives*, 1995, pp. 413–417.

[25] M. A. Rahman and O. M. Osheiba, "Performance of large line-start permanent magnet synchronous motors," *IEEE Trans. Energy Conversion*, vol. 5, pp. 211–217, Mar. 1990.

[26] A. M. Knight and C. I. McClay, "The design of high-efficiency line-start motors," *IEEE Trans. Ind. Applicat.*, vol. 36, pp. 1555–1562, Nov./Dec. 2000.

[27] B. N. Chaudhari and B. G. Fernandes, "Synchronous motor using ferrite magnets for general purpose energy efficient drive," in *Proc. IEEE Region 10 Conf. (TENCON 99)*, 1999, pp. 371–374.

[28] A. M. Knight and J. C. Salmon, "A comparison between finite element techniques when modeling single phase line-start permanent magnet motors," in *Proc. Ninth Int. Conf. Electrical Machines and Drives*, 1999, pp. 351–355.

[29] J. P. Borrelli and R. Burkhart, "New phase-sensitive technology for capacitor-start motor simplifies application," *IEEE Trans. Ind. Applicat.*, vol. 34, pp. 253–257, Mar./Apr. 1998.

[30] K. J. Tseng and S. B. Wee, "Analysis of flux distribution and core losses in interior permanent magnet motor," *IEEE Trans. Energy Conversion*, vol. 14, pp. 969–975, Dec. 1999.

[31] F. Bernal-Fernandez, A. Garcia-Cerrada, and R. Faure, "Determination of parameters in interior permanent magnet synchronous motors with iron losses without torque measurement," *IEEE Trans. Ind. Applicat.*, vol. 37, pp. 1265–1272, Sept./Oct. 2001.

[32] C. R. Steen, "Direct axis aiding permanent magnets for a laminated synchronous motor rotor," U.S. Patent 4 139 790, Feb. 1979.

[33] G. B. Kliman, M. A. Preston, and D. W. Jones, "Permanent magnet line start motor having magnets outside the starting cage," U.S. Patent 5 548 172, August 1996.

[34] K. Miyashita *et al.*, "Stress protection for permanent magnet type synchronous motor," U.S. Patent 4 144 469, August 1977.

[35] K. Mikulic, "Rotor lamination for an AC permanent magnet synchronous motor," U.S. Patent 5 097 166, Sept. 1990.

T. J. E. Miller (M'74–SM'82–F'96) is a native of Wigan, U.K. He received the B.Sc. degree from the University of Glasgow, Glasgow, U.K., and the Ph.D. degree from the University of Leeds, Leeds, U.K.

He is Professor of Electrical Power Engineering and founder and Director of the SPEED Consortium at the University of Glasgow, Glasgow, U.K. He is the author of over 100 publications in the fields of motors, drives, power systems, and power electronics, including seven books. From 1979 to 1986, he was an Electrical Engineer and Program Manager at GE Research and Development, Schenectady, NY, and his industrial experience includes periods with GEC (UK), British Gas, International Research and Development, and a student apprenticeship with Tube Investments Ltd.

Prof. Miller is a Fellow of the Institution of Electrical Engineers, U.K.

Mircea Popescu (S'98–M'99) was born in Bucharest, Romania, in 1959. He received the B.Sc. degree in statistics and economics from the Academy of Economical Studies, Bucharest, Romania, in 1992, and the M.Eng. and Ph.D. degrees in electrical engineering from the University "Politehnica" Bucharest, Bucharest, Romania, in 1984 and 1999, respectively.

From 1984 to 1986, he was involved in dc drives design and quality testing at "Electrothenica" S.A. Bucharest. From 1986 to 1997, he worked in industrial research and development at the Research Institute for Electrical Machines (ICPE-ME), Bucharest, Romania, as a Project Manager. From 1991 to 1997, he cooperated as a Visiting Assistant Professor with the Electrical Engineering Faculty, Electrical Drives and Machines Department, University "Politehnica" Bucharest. From 1997 to 2000, he was a Research Scientist with the Electromechanics Laboratory, Helsinki University of Technology, Espoo, Finland. He is currently with the SPEED Laboratory, Glasgow University, Glasgow, U.K., as a Research Associate.

Calum Cossar was born in Hamilton, U.K., in 1962. He received the B.Sc. (Hons.) degree in electronics and electrical engineering from the University of Glasgow, Glasgow, U.K., in 1983.

From 1983 to 1988, he was with Ferranti plc, Edinburgh, U.K., where he worked on the design of high-speed digital signal processing for airborne radar applications. In 1988, he joined the SPEED Laboratory, Department of Electronics and Electrical Engineering, University of Glasgow, as a Research Assistant. He became a Research Technologist and has been involved in research and development into the implementation of switched reluctance control.

Malcolm I. McGilp was born in Helensburgh, U.K., in 1965. He received the B.Eng. (Hons.) degree in electronic systems and microcomputer engineering from the University of Glasgow, Glasgow, U.K., in 1987.

Since graduating, he has been with the SPEED Laboratory, University of Glasgow, first as a Research Assistant from 1987 to 1996 and as a Research Associate since then. He is responsible for the software architecture of the SPEED motor design software and has developed the interface and user facilities which allow it to be easy to learn and integrate with other PC-based software.

Giovanni Strappazzon graduated from the Faculty of Electrical Engineering, Padua University, Padua, Italy, in 1998, on the basis of a dissertation about analysis of small induction motors for the optimization in the design of electrical motors.

He worked shortly for a factory that makes small synchronous motors mainly for aquarium pumps. Since the beginning of 2001, he has been a Researcher on innovative motors for ACC Compressors, Pordenone, Italy.

Mr. Strappazzon won an award as a Researcher in the Department of Electrical Engineering, Padua University, in 1999.

Nicola Trivillin was born in Pordenone, Italy, in 1970. He received the "Laurea" degree in electrical engineering from Padua University, Padua, Italy, in 1995, with a thesis on finite-element analysis of a single-phase induction motor with auxiliary phase.

He joined the R&D Department of ACC Compressors, Pordenone, Italy, as an Electric Motor Specialist, and is currently Manager of the Electrical Competence Center.

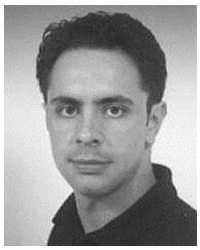

Roberto Santarossa was born in Pordenone, Italy, in 1969. He received the degree in electrical engineering from the University of Padua, Padua, Italy, in 1996, with a thesis about voltage stability of a large electric power system.

Since 1997, he has been with ACC Compressors, Pordenone, Italy, where he is currently an Electric Motor Designer, dealing with design and development of fractional horsepower motors.